nature physics

LETTERS

PUBLISHED ONLINE: 14 DECEMBER 2008; CORRECTED ONLINE: 15 DECEMBER 2008 | DOI: 10.1038/NPHYS1154

Nonlinear response of the vacuum Rabi resonance

Lev S. Bishop[1], J. M. Chow[1], Jens Koch[1], A. A. Houck[1], M. H. Devoret[1], E. Thuneberg[2], S. M. Girvin[1] and R. J. Schoelkopf[1]*

On the level of single atoms and photons, the coupling between atoms and the electromagnetic field is typically very weak. By using a cavity to confine the field, the strength of this interaction can be increased by many orders of magnitude, to a point where it dominates over any dissipative process. This strong-coupling regime of cavity quantum electrodynamics[1,2] has been reached for real atoms in optical cavities[3], and for artificial atoms in circuit quantum electrodynamics[4] and quantum dot systems[5,6]. A signature of strong coupling is the splitting of the cavity transmission peak into a pair of resolvable peaks when a single resonant atom is placed inside the cavity, an effect known as vacuum Rabi splitting. The circuit quantum electrodynamics architecture is ideally suited for going beyond this linear-response effect. Here, we show that increasing the drive power results in two unique nonlinear features in the transmitted heterodyne signal: the supersplitting of each vacuum Rabi peak into a doublet and the appearance of extra peaks with the characteristic $\sqrt{n}$ spacing of the Jaynes–Cummings ladder. These findings constitute direct evidence for the coupling between the quantized microwave field and the anharmonic spectrum of a superconducting qubit acting as an artificial atom.

Circuit quantum electrodynamics (QED) realizes the coupling between a superconducting qubit and the microwave field inside an on-chip transmission-line resonator[4,7]. The drastic reduction in mode volume for such a quasi-one-dimensional system[8,9], the recent improvement in coherence times[10] and the absence of atomic motion render circuit QED an ideal system for studying the strong-coupling limit. In the customary linear-response measurement of the transmitted microwave radiation, the vacuum Rabi splitting manifests itself as an avoided crossing between the qubit and the resonator.

It may be argued that the observation of the splitting is not yet a clear sign for quantum behaviour[11,12], because avoided crossings are also ubiquitous in classical physics. However, quantum mechanics gives rise to a distinct anharmonicity of these splittings when initializing the resonator in a higher photon Fock state: when the resonator mode is occupied by n photons, the splitting is enhanced by a factor $\sqrt{n+1}$ as compared with the vacuum Rabi situation. This anharmonicity has been observed with single atoms in both microwave[13] and optical cavities[14,15]. In circuit QED, this characteristic trait has been observed in time-domain measurements[16]. In a system similar to ours, the position of the $n=2$ peaks was recently demonstrated in a two-tone pump–probe measurement[17].

Here, we present a theoretical analysis and experimental investigation of the vacuum Rabi resonance in a circuit QED system, where we study the $\sqrt{n}$ anharmonicity up to $n=5$ by exploring the power dependence of the heterodyne transmission (see the Methods section). This type of detection is particularly simple, because it is a continuous measurement involving only a single driving frequency. We find that, surprisingly, each vacuum Rabi peak develops into a new doublet (supersplitting), which can be simply explained by the saturation of a two-level system comprising both photon and qubit degrees of freedom. For even stronger driving, a series of extra peaks due to multiphoton transitions[18,19] up the Jaynes–Cummings ladder appears, but the complete shape of the spectrum closely matches the predictions from a master equation treatment including only relaxation, dephasing and the known multilevel spectrum of the superconducting qubit. The quantitative agreement confirms the validity of the extended Jaynes–Cummings Hamiltonian for our system, rendering circuit QED an excellent tool for probing the fundamental interaction of matter and light.

We consider a system consisting of a superconducting transmon qubit[10,20] with its multiple quantum levels coupled to a single mode of a transmission-line resonator. Our arguments, however, will be general and should apply to any other realization of cavity QED with sufficiently large coupling and long enough atom coherence times. Taking into account the relatively small anharmonicity of the transmon qubit, the system is modelled in terms of an extended Jaynes–Cummings Hamiltonian including a coherent drive at frequency $\omega_d/2\pi$,

$$H = \hbar\omega_r a^\dagger a + \sum_j \hbar\omega_j |j\rangle\langle j| + \sum_j \hbar g_j \left(a|j+1\rangle\langle j| + \text{h.c.}\right) + \hbar\xi\,(a^\dagger e^{-i\omega_d t} + \text{h.c.}).$$

Here, the operator a ($a^\dagger$) annihilates (creates) a photon in the resonator mode with frequency $\omega_r/2\pi$. The energies corresponding to the transmon eigenstates are $\hbar\omega_j$ ($j=0,1,\ldots$), and they are determined by the Cooper pair box Hamiltonian[21] for given Josephson energy E_J and charging energy E_C. In the transmon regime considered here, $E_J/E_C \gg 1$, the levels form a weakly anharmonic ladder with anharmonicity $\alpha = \omega_{12} - \omega_{01} \sim -E_C/\hbar$ (where $\omega_{ij} = \omega_j - \omega_i$ is the transition frequency between levels i and j). The transmon–resonator coupling strengths are $g_j \sim g_0\sqrt{j+1}$, where $g_0/2\pi$ is the vacuum Rabi frequency. We have neglected non-nearest-neighbour terms, $|i\rangle\langle j|(a+a^\dagger)$, $i \neq j \pm 1$, because they are small in this regime[20]. We are interested in the case where the drive, the qubit and the cavity are all tuned close to the same frequency. As the drive is small, $\xi \ll \omega_d$, we have taken a rotating-wave approximation and dropped rapidly oscillating terms. The resulting energy level diagram for vanishing drive, $\xi = 0$, is schematically shown in Fig. 1.

The interaction of the cavity–transmon system with its environment enables control and measurement by means of microwave drive and detection[4,7], but also leads to decoherence.

[1]Departments of Physics and Applied Physics, Yale University, PO Box 208120, New Haven, Connecticut 06520, USA, [2]Department of Physical Sciences, University of Oulu, PO Box 3000, FI-90014, Finland. *e-mail: robert.schoelkopf@yale.edu.

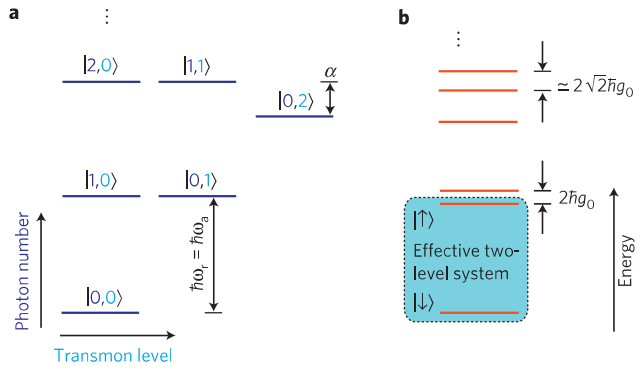

Figure 1 | Extended Jaynes–Cummings level diagram of the resonator–transmon system. a, Bare levels in the absence of coupling. The states are denoted $|n,j\rangle$ for photon number n and occupation of transmon level j. **b**, Spectrum of the system including the effects of transmon–resonator coupling. The effective two-level system relevant to describing the lower vacuum Rabi peak comprises the ground state and the antisymmetric combination of qubit and photon excitations.

The appropriate framework to capture all of these effects is a description in terms of the reduced density matrix ρ for the cavity and transmon. The Markovian master equation that governs the evolution of ρ is given by

$$\dot{\rho} = -\frac{i}{\hbar}[H,\rho]+\kappa\mathcal{D}[a]\rho+\gamma_1\mathcal{D}\Big[\sum_j \alpha_j|j\rangle\langle j+1|\Big]\rho + \frac{\gamma_\varphi}{2}\mathcal{D}\Big[\sum_j \beta_j|j\rangle\langle j|\Big]\rho, \quad (1)$$

where $\mathcal{D}[A]$ is the usual Lindblad damping superoperator defined by $\mathcal{D}[A]\rho = ([A\rho,A^\dagger]+[A,\rho A^\dagger])/2$. The three damping terms on the right-hand side model the loss of cavity photons at rate κ, the intrinsic relaxation of transmon excitations at rate γ_1, and the pure dephasing of transmon state superpositions at rate γ_φ and relative strengths α_j, β_j (see the Methods section).

The quantity of interest for detection of the vacuum Rabi splitting is the transmitted amplitude $A(\omega_d)$ of a microwave signal at frequency $\omega_d/2\pi$. Here, we use a heterodyne measurement of the field quadratures $I = V_0\langle a+a^\dagger\rangle$ and $Q = V_0\langle ia^\dagger - ia\rangle$, where V_0 is a voltage related to the gain of the experimental amplification chain. We can express the steady-state transmission amplitude as

$$A = V_0\sqrt{I^2+Q^2} = 2V_0|\langle a\rangle| = 2V_0|\mathrm{tr}(a\rho_s)|. \quad (2)$$

Our calculations thus require only the steady-state solution ρ_s of the master equation (1). We explore the transmission intensity A^2 as a function of the drive strength ξ, and compare our results to experimental data obtained for a transmon qubit in resonance with a $\omega_r/2\pi = 6.92$ GHz coplanar waveguide (CPW) resonator with coupling strength $g_0/\pi = 347$ MHz (see the Methods section for experimental details). The intensity A^2 is conveniently expressed in units of $A_1^2 = 4V_0^2$, the intensity resulting from a coherent state with a mean cavity occupancy of one photon.

In the linear-response regime, the vacuum Rabi peaks have the characteristic Lorentzian line shape. Their separation and width are given by $2g_0$ and $(\gamma_1+2\gamma_\varphi+\kappa)/2$, respectively. For our specific sample, the splitting is observed to exceed 260 linewidths, shown in Fig. 2a. Strikingly, when increasing the drive power beyond the linear-response regime, the shape of the transmission curve changes drastically as shown in Fig. 2b–f. Each vacuum Rabi peak develops a central dip and eventually supersplits into a doublet of

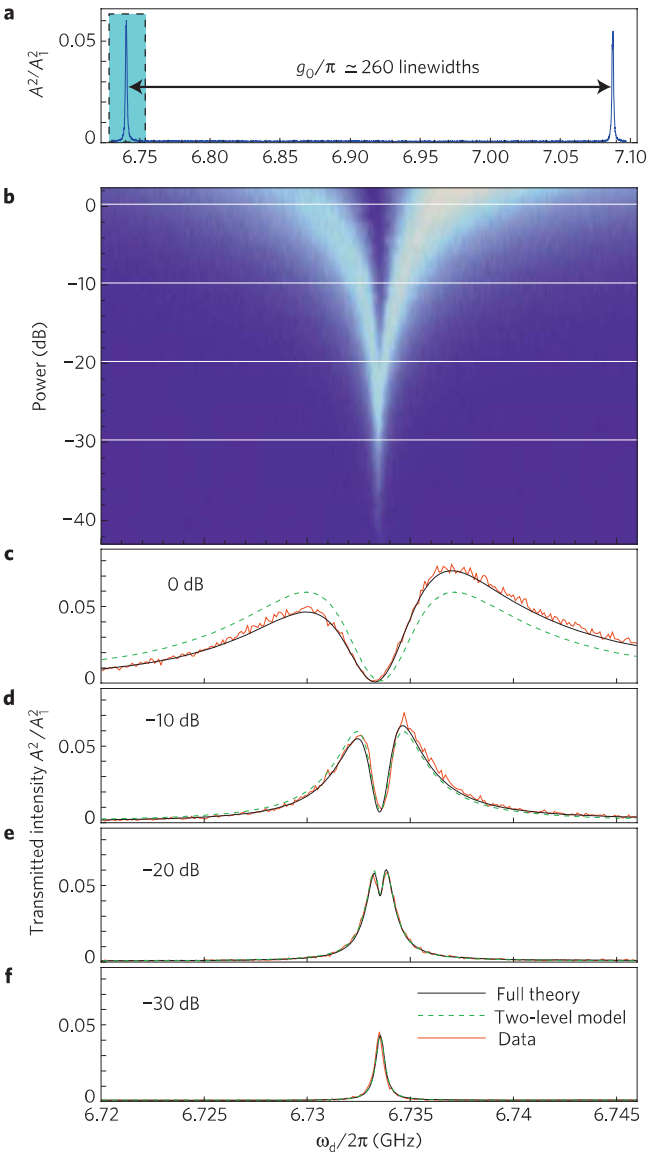

Figure 2 | Supersplitting of the vacuum Rabi resonance when probing heterodyne transmission beyond linear response. a, The experimental data are obtained with a circuit QED system in the strong-coupling regime, where the vacuum Rabi splitting is observed to exceed 260 linewidths. All plots show the heterodyne intensity A^2 in units of A_1^2. **b**, Measured intensity (colour scale) for the left vacuum Rabi peak, as a function of drive frequency and power. The plot reveals the supersplitting of a single Lorentzian into a doublet of peaks. **c–f**, Cuts for constant power at the values indicated in **b**. In linear response (**f**), the vacuum Rabi peak is Lorentzian; as the power increases, a central dip develops (**e**), leading to supersplitting of the peak (**d**) and eventually becoming asymmetric at the largest powers (**c**). The experimental data (red line) are in excellent agreement with theory (black line). The results from the two-level approximation are shown for comparison (green dashed line).

peaks. We find excellent agreement between our prediction based on equations (1) and (2) and the measured intensity.

The physics of this supersplitting can be elucidated within a reduced two-level model. In the case of the left vacuum Rabi peak, this model (represented in Fig. 1b) takes into account only the Jaynes–Cummings ground state and the antisymmetric superposition of transmon and photon excitation. (The right vacuum Rabi peak may be modelled by instead taking the symmetric superposition.) These two states, $|\downarrow\rangle = |0,0\rangle$ and $|\uparrow\rangle = (|1,0\rangle -$

$|0,1\rangle)/\sqrt{2}$, form an effective two-level system composed of both transmon and cavity degrees of freedom. Within the effective two-level subspace, the photon operators are mapped[22] to Pauli operators $a \to \Sigma_-/\sqrt{2}$, $a^\dagger \to \Sigma_+/\sqrt{2}$, so that the microwave tone acts as a drive on the effective two-level system, that is,

$$H_{\rm eff} = \frac{\hbar\Delta}{2}\Sigma_z + \frac{\hbar\Omega}{2}\Sigma_x, \qquad (3)$$

a scenario that Carmichael and co-workers[12,22] have referred to as 'dressing of dressed states'. The Hamiltonian $H_{\rm eff}$ refers to the frame rotating at the drive frequency, $\Delta = \omega_{01} - g_0 - \omega_{\rm d}$ is the detuning between the drive and the vacuum Rabi peak and $\Omega = \sqrt{2}\xi$ is the effective drive strength. With the notable exception of the recent work by Schuster *et al.*[14], previous investigations were primarily concerned with effects on photon correlations and fluorescence, as observed in photon-counting measurements[12,15]. According to the operator mapping, photon counting can be related to the measurement of $\langle\Sigma_z\rangle$, whereas detection of the heterodyne amplitude A corresponds to $|\langle\Sigma_-\rangle|$. As a result, heterodyne detection fundamentally differs from photon counting and the vacuum Rabi supersplitting is a characteristic only of heterodyne detection.

After restricting the master equation (1) to the two-level subspace, the system evolution can be expressed in terms of simple Bloch equations for the three components of the reduced density matrix $\rho = (\mathbb{1} + x\Sigma_x + y\Sigma_y + z\Sigma_z)/2$,

$$\dot{x} = -x/T_2' - \Delta y, \qquad \dot{y} = \Delta x - y/T_2' - \Omega z,$$
$$\dot{z} = \Omega y - (z+1)/T_1'.$$

(An intuitive approach ignoring dissipation and avoiding the Bloch equations is discussed in Supplementary Information, Discussion.) Here, T_1' and T_2' are the effective relaxation and dephasing times, which are related to γ_1, γ_φ and κ via $T_1'^{-1} = (\gamma_1 + \kappa)/2$ and $T_2'^{-1} = (\gamma_1 + 2\gamma_\varphi + \kappa)/4$. The usual steady-state solution of the Bloch equations for x and y gives the heterodyne amplitude

$$A = \frac{V_0 T_2' \Omega \sqrt{(\Delta^2 T_2'^2 + 1)/2}}{\Delta^2 T_2'^2 + T_1' T_2' \Omega^2 + 1}. \qquad (4)$$

This expression correctly describes the crossover from the linear response at small driving strength, $\Omega \ll (T_1' T_2')^{-1/2}$, producing a Lorentzian of width $2T_2'^{-1}$, to the doublet structure observed for strong driving. Specifically, as the drive power is increased, the response saturates and the peak broadens, until at $\Omega = (T_1' T_2')^{-1/2}$ the peak undergoes supersplitting with peak–peak separation $2T_2'^{-1}\sqrt{T_1' T_2' \Omega^2 - 1}$. The fact that we use heterodyne detection is indeed crucial for the supersplitting. It is easy to verify within the two-level approximation that photon counting always results in a Lorentzian. For photon counting, probing beyond the linear-response regime merely results in power broadening; specifically, the width of the Lorentzian is given by $2T_2'^{-1}\sqrt{T_1' T_2' \Omega^2 + 1}$ (see Supplementary Information, Fig. S4). That there is a difference between photon counting and heterodyne detection is a characteristic of a single qubit. For a many-qubit system, both types of measurement would typically give the same result, and this many-qubit nonlinear response would be rather different to the single-qubit case, developing first as a frequency pulling and eventually yielding hysteresis[23].

In Fig. 2c–f, the analytical expression (4) is plotted for comparison with the full numerical results and the experimental data. We find good agreement for low to moderate drive power, confirming that the supersplitting can be attributed to driving the vacuum Rabi transition into saturation while measuring the transmission with the heterodyne technique. For higher drive power, a left–right asymmetry appears in the true transmission spectrum, which is not reproduced by equation (4), and which is partly due to the influence of levels beyond the two-level approximation.

Higher levels of the extended Jaynes–Cummings Hamiltonian become increasingly important when the drive power is raised fur-

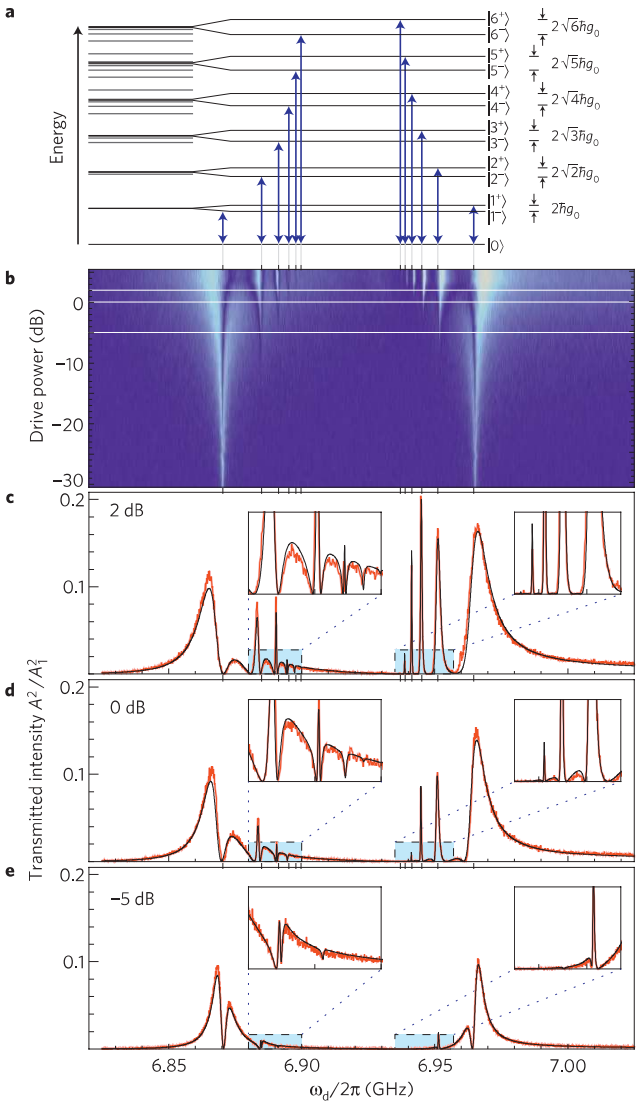

Figure 3 | Emergence of $\sqrt{n}$ peaks under strong driving of the vacuum Rabi transition. a, The extended Jaynes–Cummings energy spectrum. All levels are shown to scale in the left part of the diagram: black lines represent levels $|n,\pm\rangle \simeq (|n,0\rangle \pm |n-1,1\rangle)/\sqrt{2}$ with only small contributions from higher ($j > 1$) transmon states; grey lines represent levels with large contributions from higher transmon states. In the right part of the diagram, the $\sqrt{n}$ scaling of the splitting between the $|n,\pm\rangle$ states is exaggerated for clarity, and the transitions observed in plots **b**–**e** are indicated at the x-coordinate $E_{n\pm}/nh$ of their n-photon transition frequency from the ground state. **b**, Measured intensity (A^2, heterodyne amplitude squared) in colour scale as a function of drive frequency and power. The multiphoton transitions shown in **a** are observed at their calculated positions. **c**–**e**, Examples of cuts for constant power, at the values indicated in **b** (results from the master equation (1) in black; experimental results in red), demonstrating excellent agreement between theory and experiment, which is reinforced in the enlarged insets. Good agreement is found over the full range in drive power from −45 dB to +3 dB, for a single set of parameters (also see Supplementary Information, Movie S1).

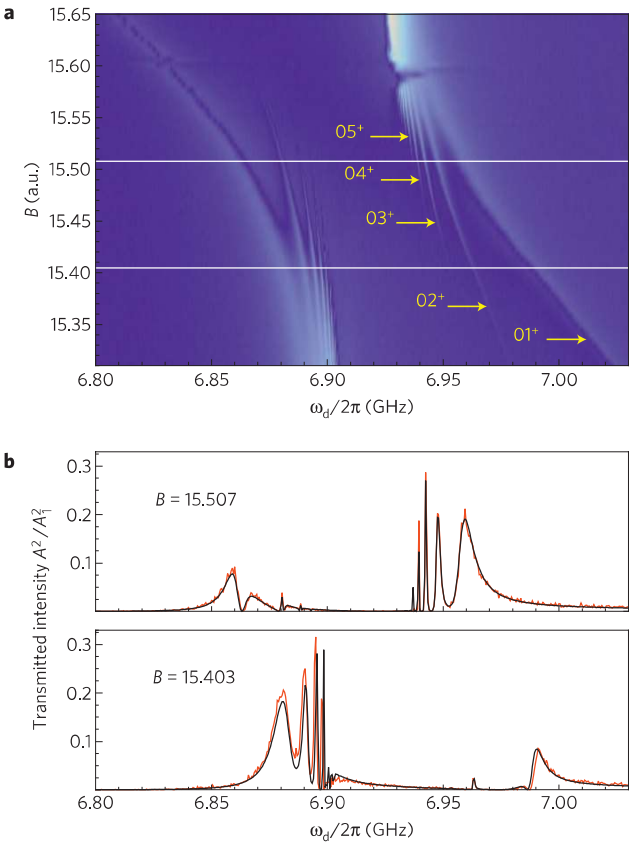

Figure 4 | Qubit–cavity avoided crossing at high drive power. Transmission measurement when tuning the qubit frequency through resonance for a drive power of +1 dB. **a**, Measured intensity as a function of drive frequency and magnetic field. As the field is increased, the qubit frequency is tuned through resonance with the cavity, and anticrossing behaviour is observed. The multiphoton transitions shown in Fig. 3a are visible. The anomaly at $B \simeq 15.59$ is most likely due to the crossing of a higher level of the second qubit present in the same cavity. **b**, Example cuts at constant magnetic field, at the values indicated in **a** (master equation results, calculated using the same parameters as for Fig. 3, are shown in black; measured results in red). (Also see Supplementary Information, Movie S2.)

ther. Figure 3 shows the emergence of extra peaks in the transmission spectrum. Each of the peaks can be uniquely identified with a multiphoton transition from the ground state to an excited Jaynes–Cummings state. For simplicity, we consider the situation where the anharmonicity α and the coupling strength g_0 are sufficiently different that mixing between higher transmon levels and the regular Jaynes–Cummings states $|n,\pm\rangle = (|n,0\rangle \pm |n-1,1\rangle)/\sqrt{2}$ is minimal for the low-excitation subspaces. Accordingly, the experiments are carried out using a different transmon qubit in the same sample, with a smaller coupling of $g_0/\pi = 94.4\,\mathrm{MHz}$ (see the Methods section). In this case, the n-photon transitions to the n-excitation subspace occur at frequencies $E_{n\pm}/nh = (\omega_r \pm n^{-1/2}g_0)/2\pi$, and thus reveal the anharmonicity of the Jaynes–Cummings ladder. The features associated with unsaturated n-photon transitions have a width set by the characteristic decay rates from the $|n,\pm\rangle$ states, $[(2n-1)\kappa+\gamma_1]/2 \simeq 1\,\mathrm{MHz}$. As the drive increases, each n-photon transition begins to saturate in turn and develop extra structure analogous to the supersplitting of the vacuum Rabi peaks. The detailed comparison between experimental data and numerical simulation in Fig. 3c–e shows superb agreement down to the narrowest features observed. (Supplementary Information, Fig. S5 shows the quadratures of the simulated spectrum.)

The possibility of multiphoton transitions at sufficiently large drive powers also affects the shape of the vacuum Rabi splitting when tuning the qubit frequency ω_{01} through resonance with the cavity, shown in Fig. 4. Instead of the simple avoided crossing commonly observed at low drive powers[4], the presence of multiphoton transitions leads to a fan-like structure where individual branches can again be identified one-to-one with the possible transitions in the Jaynes–Cummings ladder. In the experimental data of Fig. 4a, processes up to the five-photon transition are clearly visible. Detailed agreement with the theory verifies that the more general situation of non-zero detuning between the qubit and the resonator is correctly described by our model.

In summary, we have shown the supersplitting and the emergence of multiphoton transitions in the nonlinear response of the vacuum Rabi resonance, presenting both theoretical predictions and their experimental verification. This enables the observation of the characteristic $\sqrt{n}$ anharmonicity in the Jaynes–Cummings ladder in a heterodyne transmission measurement, and is direct evidence for the strong coupling between the superconducting qubit and the quantized microwave field. The high precision of agreement between predictions and experiment demonstrates the robustness of the Jaynes–Cummings physics in a circuit QED system. This opens up pathways for further investigations in quantum optics and quantum information, such as generating number-squeezed states or using multilevel quantum logic.

Methods

Theory. The modelling of the transmon follows ref. 20. Although some expressions given in the main text are asymptotic results valid only for $E_J/E_C \gg 1$, our calculations are based on a full diagonalization of the Cooper pair box Hamiltonian.

The description of the transmon–cavity system in terms of a master equation requires a model for the relaxation and dephasing of higher transmon levels. As detailed studies of the microscopic origin of the dominant relaxation and dephasing channels are still outstanding, we have chosen plausible superoperators for our master equation (1). Assuming that relaxation of higher transmon levels may arise owing to a coupling of external degrees of freedom to the charge on the superconducting island, we take the relative strengths of relaxation to be related to the coupling parameters as $\alpha_j = g_j/g_0$. Dephasing of higher levels is likely to be due to charge noise. Denoting the charge dispersion[20] of level j by $\epsilon_j = \omega_j(n_g = 0) - \omega_j(n_g = 1/2)$, we therefore take the relative dephasing strengths to be $\beta_j = 2\epsilon_j/(\epsilon_1 - \epsilon_0)$. (The normalization of α_j and β_j is chosen to allow the usual interpretation of γ_1 and γ_φ as relaxation and dephasing rates for the first two levels of the transmon spectrum.) In fact, the pure dephasing rate is sufficiently small for our qubits that we set $\gamma_\varphi = 0$. A comparison of extra simulations with auxiliary experimental results at increased temperatures enables us to place an approximate upper bound of 0.003 on the number of thermal photons in the cavity.

For the steady-state solution of equation (1), the Hilbert space is truncated to a subspace with maximum number of excitations N, using the projector $P_N = \sum_{0 \leqslant n+j \leqslant N} |n,j\rangle\langle n,j|$. In our simulations, we keep up to $N = 7$ excitations. To reach agreement with the experimentally measured signal for the strongest drive powers, it is necessary to account for a small amount ($\sim$−58 dB) of leakage of the drive past the cavity. In addition, there is a small bias introduced by measuring the intensity as the square of the I and Q quadratures, each of which is subject to noise. Accordingly, the quantity that corresponds to the experimental signal is $A^2 = |2V_0 \mathrm{tr}(a\,\rho_s) + b\xi|^2 + 2\sigma_n^2$, where b describes the leakage of the drive bypassing the cavity and σ_n is the measurement noise in each of the I and Q channels.

Fits are obtained by minimizing the mean squared deviation between experiment and calculation over the full power range, with fit parameters being b and the two scaling factors describing the attenuation and amplification for input and output signals. (In our plots, the output scaling factor is applied to the experimental data, converting them to units of A_1^2.) To obtain optimal agreement, we also make small adjustments to the system parameters γ_1, κ, g_0, ω_r, ω_{01} and E_C. These parameters are confined by separate experiments to narrow ranges, and all values used in fits are consistent within the experimental uncertainties. Once obtained, the same set of parameters was used in generating Figs 3 and 4, and Supplementary Information, Movies.

Experiment. Measurements are carried out in a dilution refrigerator at 15 mK. The sample consists of two superconducting transmon qubits[10,20], coupled to an on-chip CPW cavity. Fabrication of the sample followed the description given in ref. 10. The CPW resonator has a half-wavelength resonant frequency of $\omega_r/2\pi = 6.92\,\mathrm{GHz}$ and

a photon decay rate of $\kappa/2\pi = 300$ kHz. Transmission measurements are carried out using a heterodyne detection scheme. The transmitted radiofrequency voltage signal through the cavity is mixed down to a 1 MHz carrier signal, and then digitally mixed down to d.c. to obtain the transmitted voltage amplitude as a function of frequency. The vacuum Rabi coupling strengths for the two qubits are obtained as $g_0/\pi = 347$ MHz (qubit 1) and $g_0/\pi = 94.4$ MHz (qubit 2). Time-domain measurements of the qubits show that they are Purcell-limited and completely homogeneously broadened at their flux sweet spots[24]. The coherence times are $T_1 = 1.7\,\mu$s and $T_2 = 0.7\,\mu$s (qubit 1, away from the flux sweet spot) and $T_1 = 1.4\,\mu$s and $T_2 = 2.8\,\mu$s (qubit 2, at flux sweet spot). The charging energies of the two qubits are measured to be $E_C/h = 400$ MHz and $E_C/h = 340$ MHz. (See Supplementary Information, Methods, for further details.)

Received 17 June 2008; accepted 10 November 2008; published online 14 December 2008

References

1. Raimond, J. M., Brune, M. & Haroche, S. Manipulating quantum entanglement with atoms and photons in a cavity. *Rev. Mod. Phys.* **73**, 565–582 (2001).
2. Miller, R. *et al.* Trapped atoms in cavity QED: Coupling quantized light and matter. *J. Phys. B* **38**, S551–S565 (2005).
3. Thompson, R. J., Rempe, G. & Kimble, H. J. Observation of normal-mode splitting for an atom in an optical cavity. *Phys. Rev. Lett.* **68**, 1132–1135 (1992).
4. Wallraff, A. *et al.* Strong coupling of a single photon to a superconducting qubit using circuit quantum electrodynamics. *Nature* **431**, 162–167 (2004).
5. Reithmaier, J. P. *et al.* Strong coupling in a single quantum dot-semiconductor microcavity system. *Nature* **432**, 197–200 (2004).
6. Yoshie, T. *et al.* Vacuum Rabi splitting with a single quantum dot in a photonic crystal nanocavity. *Nature* **432**, 200–203 (2004).
7. Blais, A., Huang, R.-S., Wallraff, A., Girvin, S. M. & Schoelkopf, R. J. Cavity quantum electrodynamics for superconducting electrical circuits: An architecture for quantum computation. *Phys. Rev. A* **69**, 062320 (2004).
8. Devoret, M., Girvin, S. & Schoelkopf, R. J. Circuit-QED: How strong can the coupling between a Josephson junction atom and a transmission line resonator be? *Ann. Phys. (Leipz.)* **16**, 767–779 (2007).
9. Schoelkopf, R. J. & Girvin, S. M. Wiring up quantum systems. *Nature* **451**, 664–669 (2008).
10. Schreier, J. A. *et al.* Suppressing charge noise decoherence in superconducting charge qubits. *Phys. Rev. B* **77**, 180502 (2008).
11. Zhu, Y. *et al.* Vacuum Rabi splitting as a feature of linear-dispersion theory: Analysis and experimental observations. *Phys. Rev. Lett.* **64**, 2499–2502 (1990).
12. Tian, L. & Carmichael, H. J. Quantum trajectory simulations of the two-state behavior of an optical cavity containing one atom. *Phys. Rev. A* **46**, R6801–R6804 (1992).
13. Brune, M. *et al.* Quantum Rabi oscillation: A direct test of field quantization in a cavity. *Phys. Rev. Lett.* **76**, 1800–1803 (1996).
14. Schuster, I. *et al.* Nonlinear spectroscopy of photons bound to one atom. *Nature Phys.* **4**, 382–385 (2008).
15. Birnbaum, K. M. *et al.* Photon blockade in an optical cavity with one trapped atom. *Nature* **436**, 87–90 (2005).
16. Hofheinz, M. *et al.* Generation of Fock states in a superconducting quantum circuit. *Nature* **454**, 310–314 (2008).
17. Fink, J. M. *et al.* Climbing the Jaynes–Cummings ladder and observing its nonlinearity in a cavity QED system. *Nature* **454**, 315–318 (2008).
18. Carmichael, H. J., Tian, L., Ren, W. & Alsing, P. in *Cavity Quantum Electrodynamics* (ed. Berman, P. R.) 381–423 (Academic, 1994).
19. Deppe, F. *et al.* Two-photon probe of the Jaynes–Cummings model and controlled symmetry breaking in circuit QED. *Nature Phys.* **4**, 686–691 (2008).
20. Koch, J. *et al.* Charge-insensitive qubit design derived from the Cooper pair box. *Phys. Rev. A* **76**, 042319 (2007).
21. Bouchiat, V., Vion, D., Joyez, P, Esteve, D. & Devoret, M. H. Quantum coherence with a single cooper pair. *Phys. Scr. T* **76**, 165–170 (1998).
22. Carmichael, H. J. *Statistical Methods in Quantum Optics 2: Non-Classical Fields* (Springer, 2008).
23. Gripp, J., Mielke, S. L., Orozco, L. A. & Carmichael, H. J. Anharmonicity of the vacuum Rabi peaks in a many-atom system. *Phys. Rev. A* **54**, R3746–R3749 (1996).
24. Houck, A. A. *et al.* Controlling the spontaneous emission of a superconducting transmon qubit. *Phys. Rev. Lett.* **101**, 080502 (2008).

Acknowledgements

This work has been supported by Yale University via a Quantum Information and Mesoscopic Physics Fellowship (A.A.H., J.K.), the LPS/NSA-ARO grant W911NF-05-1-0365, NSF grants DMR-0653377, DMR-0603369 and PHY-0653073 and by the Academy of Finland. We thank J. Gambetta, A. Blais and A. Wallraff for helpful discussions, and L. Frunzio and B. Johnson for fabrication of the sample.

Author contributions

J.M.C. led the experimental effort. L.S.B. and J.K. carried out the calculations and did most of the writing. A.A.H. gave technical support and conceptual advice. E.T. contributed to the early theory. M.H.D., S.M.G. and R.J.S. provided support and supervised the project.

Additional information

Supplementary Information accompanies this paper on www.nature.com/naturephysics. Reprints and permissions information is available online at http://npg.nature.com/reprintsandpermissions. Correspondence and requests for materials should be addressed to R.J.S.